The importance of realistic plasma filament waveforms for the study of resonant wave-filament interactions in tokamak edge plasmas

W. Tierens,[1, a)] W. Zhang,[1] P. Manz,[1] EUROfusion MST1 Team,[2] and ASDEX Upgrade Team[3]
[1)] *Max Planck Institute of Plasma Physics, D-85748 Garching, Germany*
[2)] *See B. Labit et al 2019 Nucl. Fusion 59 086020*
[3)] *See H. Meyer et al. 2019 Nucl. Fusion 59 112014*

(Dated: 22 April 2020)

Recently, an analytical solution for plane wave scattering at density filaments in magnetized plasma was derived[1], from which conclusions were drawn regarding the possibility of resonant wave-filament interactions[2] between electromagnetic waves in the Ion Cyclotron Range of Frequencies and density filaments in tokamak edge plasmas. This analytical solution relies on several strongly simplified assumptions, such as a constant background density and a discontinuous density step at the filament surface. In this work we numerically investigate to what extent conclusions based on this analytical solution remain qualitatively true in more realistic scenarios.

I. INTRODUCTION

In isotropic media, the scattering of electromagnetic plane waves at perfectly conducting cylinders or spheres has been well-understood since the early 1900s, when Gustav Mie derived an analytical solution of Maxwell's equations for these cases[3], a solution now known as the Mie series. More recently, the Mie series was generalized to anisotropic media, in particular to magnetized cold plasmas[1], in which plane waves can scatter at naturally occurring near-cylindrical "filaments" whose density differs from that of the surrounding plasma. Here and throughout this work, by "filament" we mean those small filaments that are extremely common[4,5] even in L-mode or ELM-free H-mode, we do not primarily discuss the larger filaments associated with ELMs, although we expect much of our conclusions to apply to those as well.

From this Mie series in magnetized plasma, or from simpler approximate solutions that neglect some of the wave modes that exist in the plasma[6], some nontrivial conclusions can be drawn regarding the behaviour of radiofrequency (RF) electromagnetic waves in tokamak edge plasmas and the parallel transport of RF power. Ram et al[1] pointed out circumstances in which the filament "behaves like a transmission line with power flowing in its interior" (i.e. in the parallel direction), a phenomenon that was also observed numerically in 3D Finite Element simulations[7]. Extreme versions of this phenomenon are sometimes described as "mode conversion resonances"[6] because the mode conversion can be resonant i.e. the mode-converted wave fields have diverging amplitude, or as "wave-filament bound states" because an electromagnetic wave can be "bound" to the filament and constrained to move along it[2,6]. This phenomenon may play a role in the experimentally observed parallel loss of RF power on some magnetically confined fusion devices[2,8].

It is natural to ask whether such predictions derived from the Mie series will actually occur in more realistic circumstances, or if they are mere mathematical artifacts arising from the physically unrealistic premises that underlie the Mie series, such as

1. The jump between the background density and filament density is a discontinuous step function.
2. The background density is spatially constant.
3. The filament density is spatially constant.
4. The confining magnetic field is spatially constant, in both direction and magnitude.
5. The filament cross section is precisely circular.
6. The filament is precisely aligned with the confining magnetic field. This premise can be relaxed in the analytic solution[9].
7. The plasma is collisionless. It is almost certainly possible to relax this premise in the analytic solution, but this has not, to our knowledge, been done.

In this paper we will use 2D Finite Element simulations to solve the wave equation in cold plasma around a filament. Then, we can compare the results with those obtained using the analytical Mie series, and see to what extent the conclusions drawn from the Mie series remain qualitatively true as we relax these unrealistic premises. We will focus in particular on premises 1-3 and to a lesser extent 5, and consider more realistic density profiles instead.

In section II, we discuss more realistic plasma filament waveforms. In section III, we give details of the Finite Element approach. The main results are in section IV, and the conclusion is in section V.

II. THE DENSITY PROFILE OF FILAMENTS IN THE EDGE PLASMA

A. Shape

The Mie series requires a density of the form

$$n = \begin{cases} n_B & r > r_F \\ n_F & r \leq r_F \end{cases} \tag{1}$$

[a)] Electronic mail: wouter.tierens@ipp.mpg.de

where r is the radial coordinate in a cylindrical coordinate system centered on the filament, r_F is the filament radius, and n_B is the background density, and n_F is the filament density. Although analytically convenient, it is clear that the discontinuous profile (1) is physically implausible.

A Gaussian profile which, in a cylindrical (r,θ) coordinate system centered on the filament, takes the form

$$n = n_B + (n_F - n_B)\exp\left(-\frac{1}{2}\left(\frac{r}{r_F}\right)^2\right) \tag{2}$$

appears more realistic, and indeed it is the solution of a particular idealized limit of the theory of blob transport in the Scrape-Off Layer[10,11]. In (2), we identified the filament radius with the standard deviation of the Gaussian.

We will also consider generalized Gaussians

$$n = n_B + (n_F - n_B)\exp\left(-\frac{1}{2}\left(\frac{r}{r_F}\right)^\beta\right) \tag{3}$$

where the exponent β controls the steepness of the density gradient, and indeed in the $\beta \to \infty$ limit we recover (1).

In experiments a steep leading edge and a less steep trailing edge is observed[12,13]. We will now construct an ansatz for the 2D density filament waveform that is compatible with this observation, an expression describing the filament in figure 1. The experimental observations are well-approximated by a two-sided piecewise exponential, a shape sometimes known as an asymmetric Laplace distribution[14]:

$$n(t) = n_B + (n_F - n_B)\begin{cases}\exp((t-t_F)/\tau_r) & t < t_F \\ \exp(-(t-t_F)/\tau_f) & t \geq t_F\end{cases} \tag{4}$$

where the density peaks at $t = t_F$. There is a short "rising time" τ_r and a longer "falling time" τ_f. Alternatively[13], (4) may be parametrized by a single time scale $\tau = \tau_r + \tau_f$ and a "pulse asymmetry parameter" $\lambda \in [0,1]$, such that $\tau_r = \lambda\tau$ and $\tau_f = (1-\lambda)\tau$.

Assuming the filament moves outward more-or-less rigidly, the wave form of the density perturbation also exhibits the form described by (4) in the radial direction. For a filament at $x = x_F$:

$$n(x) = n_b + (n_F - n_B)\begin{cases}\exp((x-x_F)/\delta_r) & x < x_F \\ \exp(-(x-x_F)/\delta_f) & x \geq x_F\end{cases} \tag{5}$$

We take the x axis in the tokamak's radial direction (increasing in the direction of the plasma, the antenna is to the left, the plasma is to the right), so the outward-moving filament has a short "rising distance" δ_r at $x < x_F$ on the side of the tokamak edge, and a longer "falling distance" δ_f at $x \geq x_F$ on the side of the core plasma. For the purposes of this paper, we need a 2D profile for the near-circular "blob" filament cross section in the radial-poloidal plane, so we generalize (5) as follows, in a cylindrical (r,θ) coordinate system centered on the filament:

$$n_{2D} = n_B + (n_F - n_B)\begin{cases} g(r_F,\theta)\exp(f(\theta)(r-r_F)) & r > r_F \\ g(r,\theta) & r \leq r_F\end{cases} \tag{6}$$

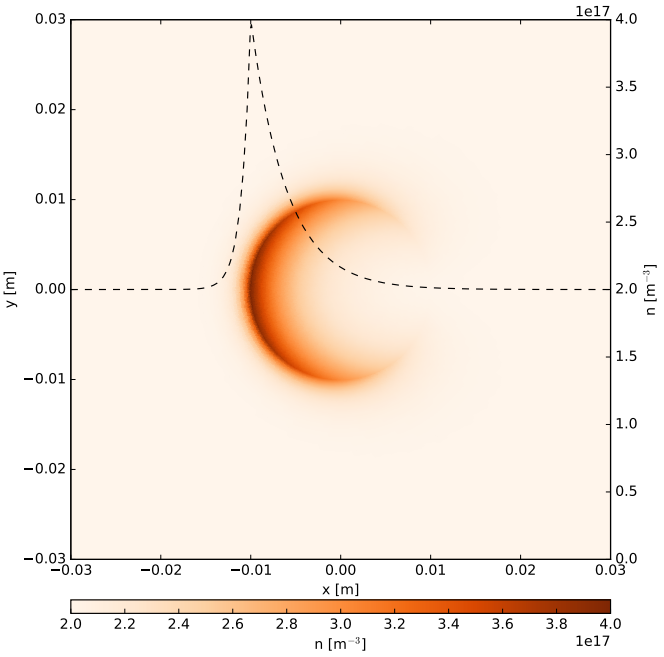

FIG. 1. A density profile of the form (6), on a constant background. Parameters are $r_F = 1\text{cm}$, $\frac{\delta_r}{r_F} = 0.1$, $\frac{\delta_F}{r_F} = 0.4$. The black dashed curve is the "cross section" along $y = 0$, which by construction has the piecewise exponential form (5). The filament is moving leftward.

where

$$f(\theta) = -\frac{\cos^2(\theta/2)}{\delta_f} - \frac{\sin^2(\theta/2)}{\delta_r} \tag{7}$$

$$g(r,\theta) = \cos^2(\theta/2)\exp\left(\frac{-r-r_F}{\delta_f}\right) + \sin^2(\theta/2)\exp\left(\frac{r-r_F}{\delta_f}\right) \tag{8}$$

Along the horizontal axis, i.e. where $\theta = 0$ or $\theta = \pi$, (6) by construction reduces to (5), with $(r = r_F, \theta = 0)$ in (6) corresponding to $x = x_F$ in (5). Furthermore, (6) is everywhere continuous, and only at $r = r_F$ is its derivative discontinuous. Maxwell's equations do not have special boundary conditions at discontinuities in the derivative of material parameters, only at discontinuities in the material parameters themselves, so we do not expect a discontinuous derivative to give rise to physically implausible behaviour. Indeed, in the results we will not find a single phenomenon that is unique to filaments of the form (6), all phenomena of interest occur also for C^∞ Gaussian filaments. Even so, appendix A details how a generalisation of (6) with continuous derivatives can be constructed.

A density profile of the form (6) is shown in figure 1. Indeed, it is localized near a circle and has the desired piecewise exponential cross section along the horizontal axis. Further evidence for the suitability of (6) as an ansatz for the filament density profile is its similarity to filament densities obtained from sophisticated edge MHD simulations[5,15–17]. In principle the filament radius r_F, rising distance δ_r and falling distance δ_f are completely independent in this formulation (even the

$\frac{\delta_f}{r_F} \to \infty$ limit makes sense), but, recalling the pulse asymmetry parameter λ, we may reasonably assume

$$r_F = \delta_r + \delta_f \tag{9}$$
$$\delta_r = \lambda r_F \tag{10}$$
$$\delta_f = (1-\lambda) r_F \tag{11}$$

For completeness, let us also mention that filament density profiles of the form

$$n = n_B + (n_F - n_B) \begin{cases} 1 & r < r_F \\ \frac{\cos\left(\pi \frac{r-r_F}{dr}\right)+1}{2} & r_F \le r < r_F + dr \\ 0 & r_F + dr \le r \end{cases} \tag{12}$$

where the cosine provides a continuously differentiable interpolation between a constant filament density at $r < r_F$ and a constant background density at $r \ge r_F + dr$ over a length scale dr, have been used in calculations of LH and ECRF wave scattering at filaments[18], but we will not consider densities of this form.

B. Amplitude

On ASDEX Upgrade, $\frac{n_F - n_B}{n_B}$ is measured in experiments[19], and rarely takes values greater than $\frac{n_F - n_B}{n_B} \approx 1$. On many other machines, the distribution of $\frac{n - <n>}{\sigma_n}$ is often remarkably well-described by a gamma distribution[12]

$$P\left(\frac{n - <n>}{\sigma_n}\right) = \frac{\gamma^{1/2}}{\Gamma(\gamma)} \left(\gamma + \gamma^{1/2} \frac{n - <n>}{\sigma_n}\right)^{\gamma-1} \cdot \exp\left(-\gamma - \gamma^{1/2} \frac{n - <n>}{\sigma_n}\right) \tag{13}$$

where n is the instantaneous density, to be identified with n_F, $< n >$ the time-averaged mean density, to be identified with n_B, and σ_n the standard deviation of n as it turbulently fluctuates over time. The so-called "intermittency parameter" γ is $\gamma = \frac{<n>^2}{\sigma_n^2}$, and typically $1 < \gamma < 10$, depending on the tokamak and on the location within the tokamak. The cumulative distribution function corresponding to (13) is

$$P\left(\frac{n_F}{n_B} > x\right) = \frac{\Gamma(\gamma, \gamma x)}{\Gamma(\gamma)} \equiv \frac{\int_{\gamma x}^{\infty} t^{\gamma-1} e^{-t} dt}{\int_0^{\infty} t^{\gamma-1} e^{-t} dt} \tag{14}$$

Several figures in this paper (figures 10,11,14 and 15) show quantities as a function of $\frac{n_F}{n_B}$. In these figures, we also show (14) on the secondary x axis (with $\gamma = 4$, within the observed range of this parameter on both AUG and NSTX), to emphasize that $\frac{n_F}{n_B}$ closer to 1 are more likely to occur in reality than larger $\frac{n_F}{n_B}$.

C. Background

For the background density n_B in the Scrape-off Layer (SOL), we will use either a constant or an exponential

$$n_B = n_{B,0} \exp(x/\Delta) \tag{15}$$

where Δ is the decay length for the SOL density, and $n_{B,0}$ the density at $x = 0$, i.e. at the radial location of the center of the filament. For numerical reasons we will avoid the Lower Hybrid resonance[20] in our simulation domain, so we impose a minimum density $n_{B,\min}$:

$$n_B = n_{B,\min} + (n_{B,0} - n_{B,\min}) \exp(x/\Delta) \tag{16}$$

In reality, most of the edge plasma is beyond the Lower Hybrid resonance, which occurs at $n \approx 5 \cdot 10^{16}$ in the dispersion relations in figures 3 and 6, so this assumption is not excessively restrictive. Green et al[21] even argue that the density in NSTX is nowhere below the density of the Lower hybrid resonance, nowhere so low as to allow propagating Slow Waves. In earlier work[2], we identified variety of resonant ICRF wave-filament interactions, and in this paper, we focus on those we believe to be of greatest practical relevance: those that occur where the background density is dense enough for the Slow Wave to be evanescent, and the filament is denser than the background. It is possible that, in other physical scenarios, other resonances become relevant, such as the ones that exist where the Slow Wave is propagating in the background, but those will not be considered in this paper.

In equations (2), (3) and (6), we wrote

$$n = n_B + (n_F - n_B) f(r, \theta) \tag{17}$$

where $f(r,\theta)$ is some expression for the shape of the filament density with a maximum value of 1. When n_B is x-dependent, $n_B = n_B(x)$, we mean

$$n(r,\theta) = n_B(r\cos(\theta)) + \underbrace{(n_F - n_B(0))}_{\text{constant}} f(r,\theta) \tag{18}$$

that is, we always multiply the filament density, whether Gaussian or of the form (6), by a constant (x-independent) amplitude factor before adding it to the possibly x-dependent background $n_B(x)$. We will usually parametrize the filament density not by n_F, but by $\frac{n_F}{n_B}$ i.e. by $\frac{n_F}{n_B(0)}$

$$n(r,\theta) = n_B(r\cos(\theta)) + \left(\frac{n_F}{n_B(0)} - 1\right) n_B(0) f(r,\theta) \tag{19}$$

III. DESCRIPTION OF THE 2D FINITE ELEMENT DISCRETISATION

We make use of the commercial Finite Element solver COMSOL[22], which is capable of solving[18,23–25] the electromagnetic wave equations in collisionless cold magnetized plasma[26]

$$\nabla \times \nabla \times \vec{E} + \frac{\omega^2}{c^2} \begin{bmatrix} \varepsilon_\perp & -i\varepsilon_\times & 0 \\ i\varepsilon_\times & \varepsilon_\perp & 0 \\ 0 & 0 & \varepsilon_\parallel \end{bmatrix} \vec{E} = 0 \tag{20}$$

provided the user manually specifies the elements $\varepsilon_\perp, \varepsilon_\times, \varepsilon_\parallel$ of the cold plasma dielectric tensor, their density-dependence[26], and their modified form where an absorbing boundary layer, or PML, is required[27].

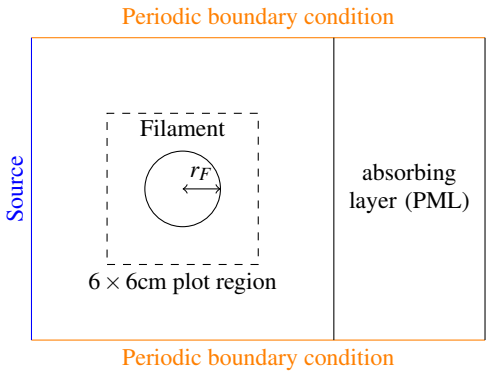

FIG. 2. 2D simulation domain. Filament and plot region not drawn to scale. The main simulation domain, not counting the PML, is 30×30cm.

We use a 2D (radial-vertical + imposed $k_\parallel$ in the toroidal direction) simulation domain as shown in figure 2. The filament has radius r_F of typically $r_F = 1$cm and is centered at $(0,0)$ in the simulation's coordinate system. At the left is the antenna, where we impose $E_y = 1$V/m on the boundary as a source condition (an unrealistically low value, but the physics is linear, so we can just multiply the results by 10^3 or 10^4 if required). On the right is the core plasma, approximated by a PML. This is similar to the configuration used in[18].

This approach allows us to resolve the region around the filament surface sufficiently densely. It is well known that the wave equation (20) gives rise to two distinct wave modes[26], known in the Ion Cyclotron Range of Frequencies (ICRF) as the Fast Wave (FW) and the Slow Wave (SW). In the region around the filament, mode conversion from the incident Fast Wave to the Slow Wave[2,26] may occur. The latter is evanescent for ICRF waves in typical tokamak edge plasma conditions, with evanescence length on the order of millimeters, hence the need to use a mesh with sub-millimetric spatial resolution, which is much less computationally demanding[7] in 2D vs. in 3D (see figure 7 for a particularly striking example of very short-wavelength phenomena at the filament interface).

In most figures in this paper we will not show the whole simulation domain, but only a 6×6cm region around the filament. This is the "plot region" which is shown as a dashed square, not to scale, in figure 2. The simulation domain is significantly larger, 30×30cm not counting the PML, both to avoid self-interaction due to the periodic boundary conditions, and to have enough space for the background density to become high enough that the Fast Wave becomes propagative.

IV. RESULTS

A. Influence of the filament on the $E_\parallel$ fields (generic/non-resonant examples)

In this section (IV A 1-IV A 3), we will show various filament density profiles and the $|E_\parallel|$ fields that form around them due to an incident ICRF Fast Wave (which itself has almost no $|E_\parallel|$). The point is to give the reader a more concrete idea of the type of density profiles that we are considering, and what the mode-converted fields look like. Although we expect this type of mode conversion at filaments to be extremely common (it should occur at nearly all filaments), we do not claim it is especially important during typical tokamak operation, with the exception of particular conditions under which the mode conversion is resonant, which we will discuss in section IV C.

One possible adverse effect of this mode conversion, even under generic conditions, is that increased $|E_\parallel|$ may increase sheath rectification, and thereby impurity production, where a filament intersects a plasma-facing component surface[7,28].

For ICRF wave-filament interactions,

$$\frac{2\pi}{|k_{x,FW}|} > r_F \gtrsim \frac{2\pi}{|k_{x,SW}|} \tag{21}$$

The length scale of the incident Fast Wave is on the order of several decimeter in the edge plasma, larger than the filament radius on the order of a centimeter, which in turn is larger than the length scale of the Slow Wave, on the order of several millimeter. It is because of this scale separation that and any strong interactions between the incident Fast Wave and the filament must involve mode conversion to the Slow Wave. Indeed, (22) was obtained assuming that the incident Fast Wave remains entirely unperturbed.

By choosing to plot the parallel electric field component, mostly associated with the evanescent Slow Wave, in the figures in sections (IV A 1-IV A 3), we necessarily see only fields near the filament interface, where the Slow Wave can be generated by mode conversion. Being evanescent, the Slow Wave decays away from the filament surface where it is excited.

Unlike in the analytic solution[2], we cannot decompose the numerical solution into a Slow Wave and a Fast Wave contribution. Thus, we use the common but inexact assumption that the parallel electric field is due to the Slow Wave, and if we see parallel electric fields in the presence of a filament that were not there in the unperturbed case, we take this to be evidence of mode conversion from the incident Fast Wave to the Slow Wave.

1. *ASDEX Upgrade (AUG)-like conditions*

For typical ASDEX Upgrade parameters, we use Deuterium plasma with $B_0 = 2$T, $k_\parallel = 9\text{m}^{-1}$, and $f = 36.5$MHz. Under these circumstances, the Fast Wave becomes propagative at densities above $\approx 5 \cdot 10^{18}\text{m}^{-3}$. A dispersion relation is shown in figure 3.

In figure 4, we show the mode-converted $|E_\parallel|$ for ICRF wave scattering at a filament of the form (6), on an exponential background as in (16), with $\Delta = 4$cm, $n_{B,0} = 2 \cdot 10^{17}\text{m}^{-3}$, and $n_{B,\min} = 5 \cdot 10^{16}\text{m}^{-3}$. For the filament density, $\frac{n_F}{n_B} = 2$. Here, the mode-converted $|E_\parallel|$ amplitude is maximal for the sharpest filament. Figure 5 shows a similar comparison for Gaussian filaments, with more mode conversion occurring at the sharper generalized Gaussian with $\beta = 4$, and less at the smoother true Gaussian with $\beta = 2$.

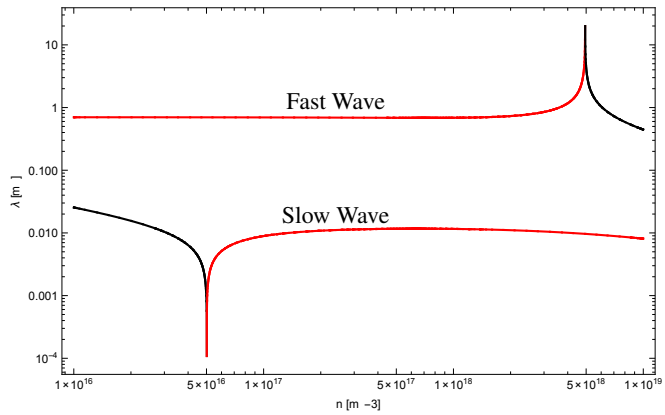

FIG. 3. Dispersion relation for plasma parameters typical in ASDEX Upgrade. Wavelengths for propagating modes in black ($\lambda = \frac{2\pi}{|k_x|}$, k_x real), length scales for evanescent modes in red ($\lambda = \frac{2\pi}{|k_x|}$, k_x imaginary).

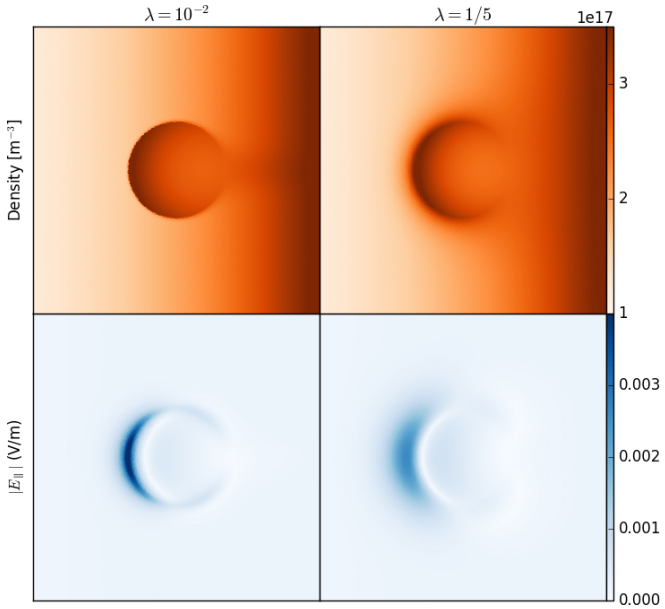

FIG. 4. n and $|E_\parallel|$ for ICRF wave scattering at density filaments of the form (6) with different pulse asymmetry parameter λ, with AUG-like RF parameters. On the left, $\lambda = 10^{-2}$, corresponding to a very small δ_r, a very sharp rise in density. On the right, $\lambda = 0.2$, which is more realistic.

2. *National Spherical Torus Experiment (NSTX)-like conditions*

For typical NSTX parameters, we use Deuterium plasma with $B_0 = 0.55$T, $k_\parallel = 3\text{m}^{-1}$, and $f = 30$MHz. Under these circumstances, the Fast Wave becomes propagative at densities above $\approx 1.5 \cdot 10^{17}\text{m}^{-3}$. A dispersion relation is shown in figure 6. The NSTX ICRF antenna is also capable of launching waves with higher $k_\parallel$, but the parallel ICRF power loss[8], a phenomenon we believe to be largely caused by resonant wave-filament interactions[2], is maximal at this low $k_\parallel$, so this

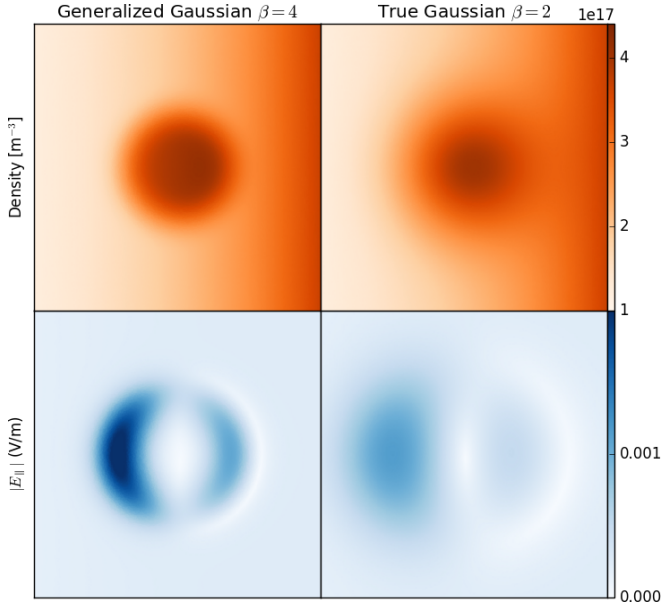

FIG. 5. n and $|E_\parallel|$ for ICRF wave scattering at generalized Gaussian (3) density filaments with different exponents β, with AUG-like RF parameters.

is the most interesting case to compare. We will revisit this point in section IV C 3.

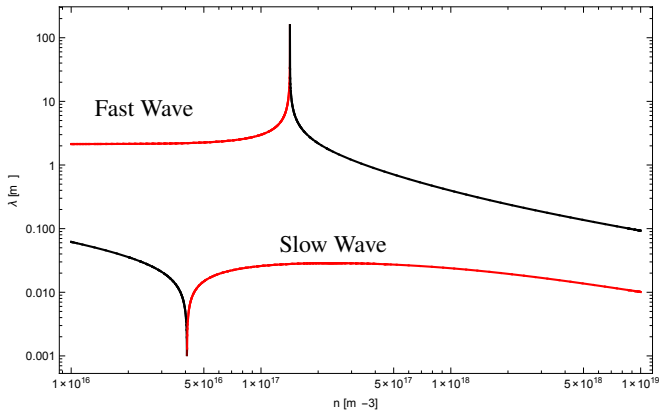

FIG. 6. Dispersion relation for plasma parameters typical in NSTX. Wavelengths for propagating modes in black ($\lambda = \frac{2\pi}{|k_x|}$, k_x real), length scales for evanescent modes in red ($\lambda = \frac{2\pi}{|k_x|}$, k_x imaginary).

In figure 7, we again show the mode-converted $|E_\parallel|$ for ICRF wave scattering at a filament. The density and filament parameters are the same as in section IV A 1. In both cases in figure 7, the mode-converted $E_\parallel$ field forms a standing wave on the steepest edge, i.e. the leading edge, of the filament. From the point of view of a cylindrical coordinate system centered on the filament, the $E_\parallel$ field has a high azimuthal mode number, something rarely seen in the Mie solution for this frequency range.

Figure 8 shows a similar comparison for Gaussian filaments. Again, a standing wave pattern forms at the sharper

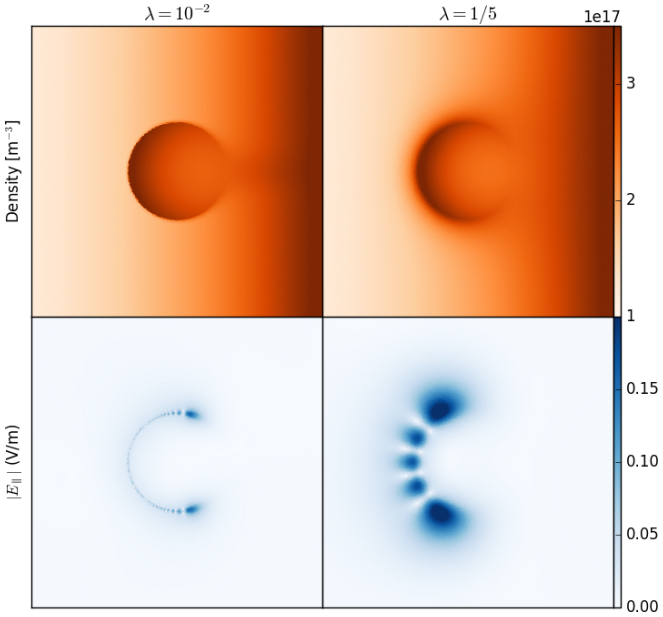

FIG. 7. n and $|E_\parallel|$ for ICRF wave scattering at density filaments of the form (6) with different pulse asymmetry parameter λ, with NSTX-like RF parameters. On the left, $\lambda = 10^{-2}$, corresponding to a very small δ_r, a very sharp rise in density. On the right, $\lambda = 0.2$, which is more realistic. In both cases, a mode-converted $E_\parallel$ standing wave pattern forms at the filament's leading edge.

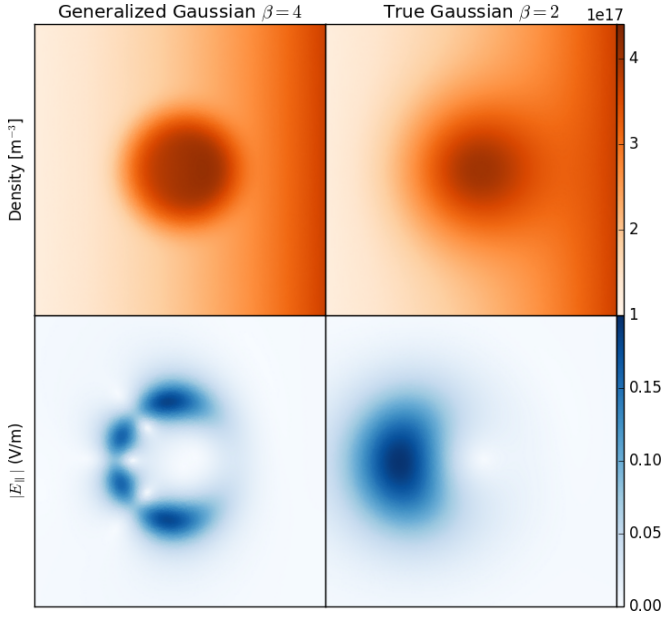

FIG. 8. n and $|E_\parallel|$ for ICRF wave scattering at generalized Gaussian (3) density filaments with different exponents β, with NSTX-like RF parameters.

($\beta = 4$) filament.

3. *Noncircular filament cross sections*

For completeness, in figure 9 we show the mode-converted $|E_\parallel|$ fields for ICRF wave scattering at elliptic filaments, obtained by simply stretching the x-coordiate by a factor 1.2 and the y-coordinate by a factor $1/1.2$ (thereby keeping the cross section surface area constant) in (2) resp (6). It is clear that the behaviour is not qualitatively different from that of circular filaments.

B. Standing surface waves

Figures 7, 8 (left) and 9 (right) show clear standing wave patterns for $|E_\parallel|$ on the filament interface. This is true for figures 4, 5, 8 (right) and 9 (left) also, but there we only see one peak of the standing wave.

We may qualitatively explain this as follows: a surface wave is supported on the filament interface, but only if the filament interface is sharp enough. At the leading (left) side of the filament, it is sharp enough to support surface waves. At the trailing (right) side, at some point the filament is no longer sharp enough to support surface waves, either due to the inherent asymmetry of the filament density itself in the case of filaments like (6), or due to the asymmetry of the background in the case of symmetric (Gaussian) filaments.

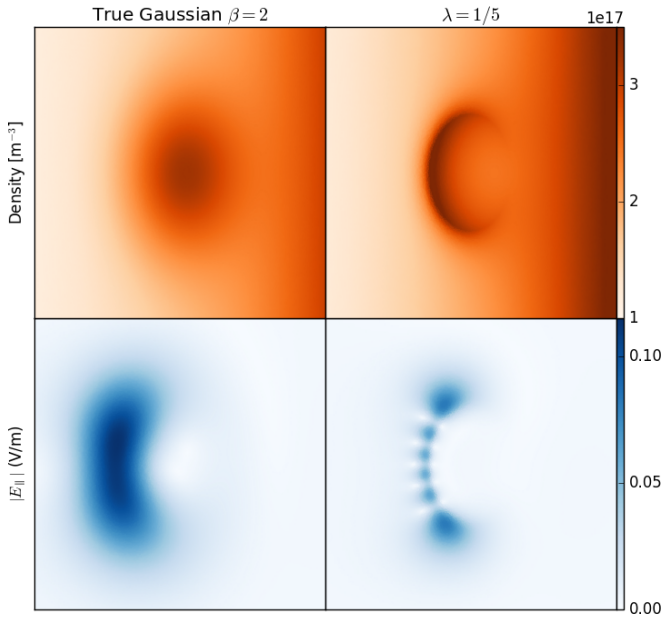

FIG. 9. n and $|E_\parallel|$ for ICRF wave scattering at a Gaussian (left) or a filament of the form (6) (right), both stretched such that the filament cross section is elliptic rather than circular. RF parameters are NSTX-like.

The dispersion relation for the surface waves must have some sharpness-dependent cutoff: after all, it is clear that surface waves exist in the infinitely sharp (discontinuous) limit, but not in the infinitely smooth (constant) limit. Thus, a standing surface wave forms on the leading edge between the two cutoffs, whose azimuthal wavelength is not solely determined by the length scales of the wave modes in the unperturbed

plasma, but also by the length scale of the density gradient at the filament interface. This is especially clear in figure 7, where the $\approx 10^{-4}$m azimuthal wavelength is shorter than even the Slow Wave evanescence length, but comparable to the filament density's rising distance $\delta_r = \frac{1}{100} r_F = 10^{-4}$m. We should expect to find mode conversion resonances where a (half-)integer number of surface wave azimuthal wavelengths fit between the cutoffs, and indeed we will see this is the case in the next section.

Lacking an expression for the sharpness-dependent dispersion relation of these surface waves, we cannot presently make this argument more precise. However, in simpler situations, like an interface between vacuum or dielectric and unmagnetized cold plasma[29,30], it is known that the behaviour of the surface waves depends crucially on the density gradient, which lends credence to the above argument.

Note that one of the classical requirements for the existence of surface waves in simple dielectrics[31] or unmagnetized plasmas[30], an abrupt sign change of ε, is not fulfilled here: none of the dielectric tensor elements $\varepsilon_\perp, \varepsilon_\parallel$ and $\varepsilon_\times$, nor any of the eigenvalues of the dielectric tensor $\varepsilon_\parallel, \varepsilon_\perp \pm \varepsilon_\times$, change sign near the filament surface at all, abruptly or otherwise.

C. Mode conversion resonances

1. *In the evanescent layer*

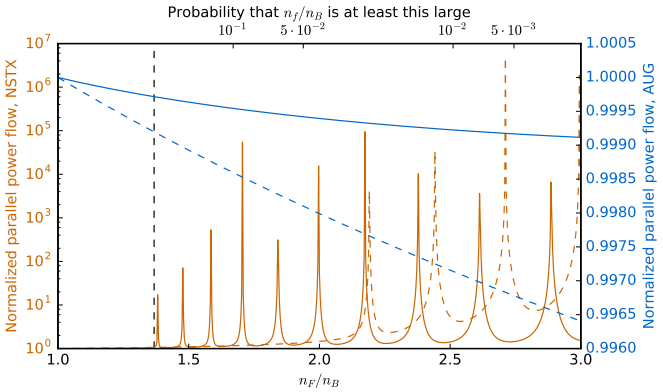

FIG. 10. Filament-integrated parallel RF power flow, normalized to that of the unperturbed case. The background is exponential as in (16), with $\Delta = 4$cm, $n_{B,0} = 10^{17}\text{m}^{-3}$, and $n_{B,\min} = 5\cdot10^{16}\text{m}^{-3}$, such that both wave modes are evanescent near the filament. The filament is either Gaussian (dashed lines) or of the form (6) (solid lines), with pulse asymmetry parameter $\lambda = 1/5$. The filament radius is $r_F = 1$cm in both cases. The secondary (top) x axis gives the cumulative distribution function for the density ratio (14). The vertical dashed line is the location of the fist resonance predicted by (22) for NSTX-like parameters. Note the vast difference between the scales of the left and right vertical axes, for NSTX-like (orange) and AUG-like (blue) parameters respectively.

In figure 10 we show a parameter scan of the parallel RF power flow in the filament, vs. $\frac{n_F}{n_B}$, with an exponential background density as in (16) with $n_{B,0} = 10^{17}\text{m}^{-3}$, a density at

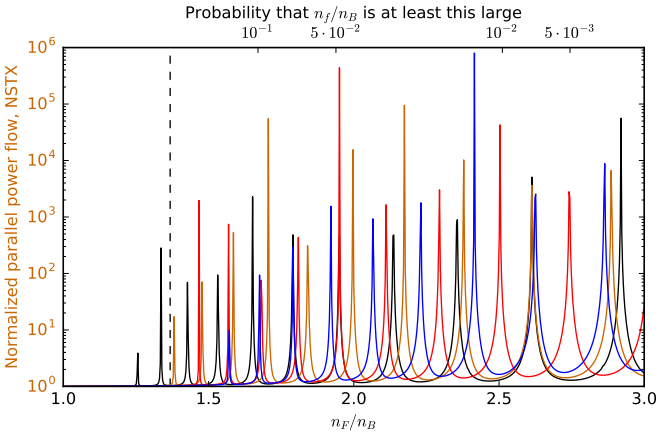

FIG. 11. Filament-integrated parallel RF power flow, normalized to that of the unperturbed case. Parameters are as in figure 10, the filament is of the form (6), with pulse asymmetry parameter $\lambda = 1/5$. The decay length Δ of the background density is $\Delta = 2$cm for the black curves, $\Delta = 4$cm for the brown curves (same as in figure 10), $\Delta = 8$cm for the red curves, and $\Delta = \infty$ (constant background) for the blue curves. The secondary (top) x axis gives the cumulative distribution function for the density ratio (14). The vertical dashed line is the location of the fist resonance predicted by (22).

which the Fast Wave is evanescent in the immediate neighbourhood of the filament, for both AUG-like and NSTX-like RF parameters. We chose this density to keep the AUG and NSTX cases as comparable as possible, but we must keep in mind that, for this background density profile, the distance between the filament and the point where the Fast Wave becomes propagative is much larger for AUG, where this happens at $n = 5\cdot10^{18}\text{m}^{-3}$ than for NSTX, where this happens at $n = 1.5\cdot10^{17}\text{m}^{-3}$.

We are interested in the possibility that a large amount of RF power may be lost in the parallel direction due to the filaments carrying RF power away from the antenna[1,2,6,7], a phenomenon known as "mode conversion resonance" or "wave-filament bound state", and more specifically in the circumstances under which this occurs. From analytical reasoning with a discontinuous density we expect[32] some of the resonances to occur at

$$\xi\left(\frac{n_F}{n_B}K_m(\xi)I_m'(\xi) - I_m(\xi)K_m'(\xi)\right) = m\frac{\omega}{\Omega_i}I_m(\xi)K_m(\xi)\left(\frac{n_F}{n_B} - 1\right) \qquad (22)$$

where $\xi = r_F k_\parallel \sqrt{\frac{m_i}{m_e}}$, the azimuthal mode number $m = \pm 1$, I_m and K_m are Bessel functions, ω is the (angular) antenna frequency and $\Omega_i = q_i B/m_i$ the ion cyclotron frequency. The vertical dashed line in figures figures 10,11,14 and 15 is the resonant $\frac{n_F}{n_B}$ predicted by (22). (22) predicts resonances close to $\frac{n_F}{n_B} = 1$ when ξ is small (small $k_\parallel$) and $\frac{\omega}{\Omega_i}$ is large (high harmonic heating), that is, operating parameters common in NSTX but uncommon in most other tokamaks. Indeed, 3D numerical studies on AUG[7] only found mode conversion resonances at unrealistically high $\frac{n_F}{n_B}$. For this and other reasons[2],

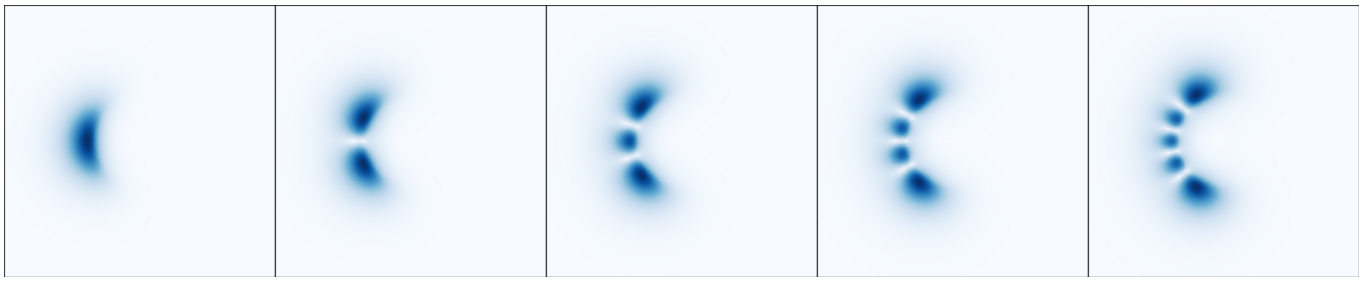

FIG. 12. $|E_\parallel|$ for the first 5 resonant peaks from figure 10, for filaments of the form (6) and NSTX-like RF parameters. This figure supports the argument of section IV B, that the mode conversion resonances are due to surface standing waves, so the nth resonance has n peaks fitting between the cutoffs.

we believe resonant wave-filament interactions to be among the factors responsible for the experimentally observed parallel RF power losses on NSTX[8]. This is the reason why we are especially interested in NSTX-like parameters.

We find that under such parameters, both Gaussian filaments and filaments given by (6) have mode conversion resonances at realistic $\frac{n_F}{n_B}$ (recall from section II B that $\frac{n_F}{n_B}$ is rarely observed to be larger than 2), and indeed there are many more such resonances than expected from (22), which predicts just one with $\frac{n_F}{n_B} > 1$ and one with $\frac{n_F}{n_B} < 1$. The smoother Gaussian filaments require larger $\frac{n_F}{n_B}$. Under AUG-like parameters, on the other hand, no mode conversion resonances occur at realistic $\frac{n_F}{n_B}$ for either type of filament. Larger amplitudes, with higher $\frac{n_F}{n_B}$ than what we consider here, are observed for ELMs. Type-I ELMs are not foreseen as a reactor relevant scenario, but a small ELM scenario[33] might be affected by mode conversion.

In figure 11 we see the influence of the background steepness i.e. of the SOL density decay length scale Δ. Steeper backgrounds (smaller Δ) do not cause mode conversion resonances to disappear, not even when Δ is as small as a filament diameter, and even cause the resonances to occur at $\frac{n_F}{n_B}$ closer to 1.

Looking at the mode-converted $|E_\parallel|$ fields corresponding to the mode conversion resonance peaks, in figure 12, we see that the nth mode conversion resonance peak has an $|E_\parallel|$ standing wave pattern with n peaks. This is exactly what we should expect from the arguments in section IV B.

2. *In the presence of propagating Fast Waves*

In earlier work[2], we briefly mentioned that propagating Fast Waves in the background plasma are a loss mechanism for resonant wave fields in the filament: energy leaks out via the propagating Fast Wave in the background plasma, and where in a background that only supports evanescent waves we find true resonances, in a background that supports propagating Fast Waves we only find high but finite "pseudo-resonances". The Fast Wave in such a scenario is shown in figure 13. Under such circumstances, the resonances should be expected to be broader and less high. Indeed, this is what we see in figure 14, where we chose the (still exponential) background density

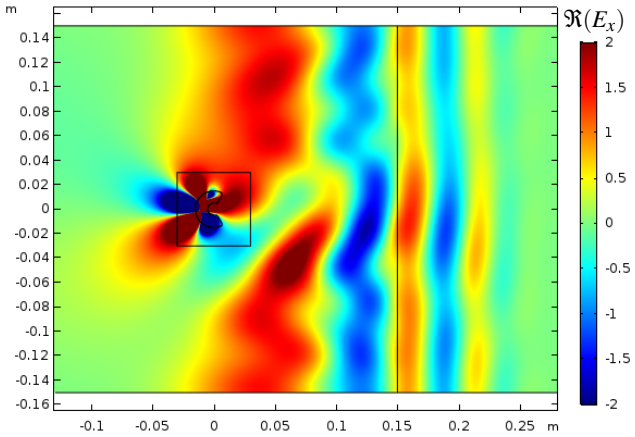

FIG. 13. Fast waves in the full simulation domain (recall figure 2). Fast waves are generated, start propagating near the filament, and are absorbed in the PML. The color indicates the radial component of the electric field, E_x. The filament density is that of the first resonant peak in figure 14.

such that Fast Waves are propagative in the immediate neighbourhood of the filament.

3. *$k_\parallel$-dependence*

Among the arguments that convince us that mode conversion resonances play a role in the parallel RF power losses on NSTX, is the correct prediction of the $k_\parallel$-dependence of this phenomenon: from (22) we expect the mode conversion resonances to occur at higher i.e. rarer $\frac{n_F}{n_B}$ for higher $k_\parallel$. Figure 15 confirms that this is still the case for more realistic densities. The few mode conversion resonances that exist for filaments of the form (6) (solid lines in figure 15) occur at higher $\frac{n_F}{n_B}$ than those at $k_\parallel = 3\mathrm{m}^{-1}$ in figure 10, and also have much lower amplitude. For Gaussian filaments (dashed lines in figure 15), no mode conversion resonances are visible at all.

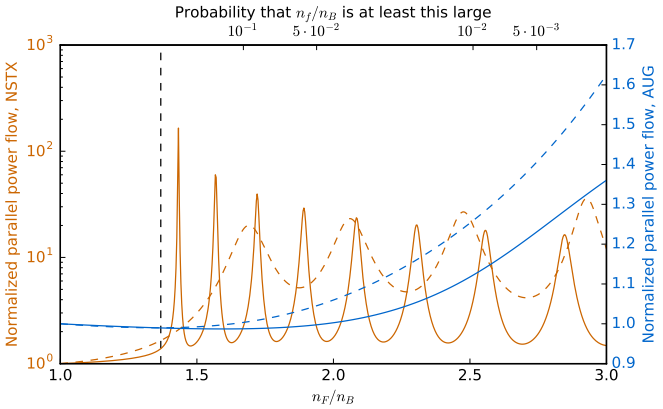

FIG. 14. Filament-integrated parallel RF power flow, normalized to that of the unperturbed case. The background is exponential as in (16), with $\Delta = 4$cm, $n_{B,\min} = 5\cdot10^{16}\mathrm{m}^{-3}$, and $n_{B,0} = 5\cdot10^{17}\mathrm{m}^{-3}$ (NSTX) or $n_{B,0} = 6\cdot10^{19}\mathrm{m}^{-3}$ (AUG), chosen such that the Fast Wave is propagative at the location of the filament for both devices, while the Slow Wave remains evanescent in the entire simulation region. The filament is either Gaussian (dashed lines) or of the form (6) (solid lines), with pulse asymmetry parameter $\lambda = 1/5$. The filament radius is $r_F = 1$cm in both cases. The secondary (top) x axis gives the cumulative distribution function for the density ratio (14). The vertical dashed line is the location of the fist resonance predicted by (22) for NSTX-like parameters. As expected, the resonance peaks are less high than in the case of figure 10, where the Fast Wave is evanescent near the filament, and there are still no resonances under AUG-like parameters.

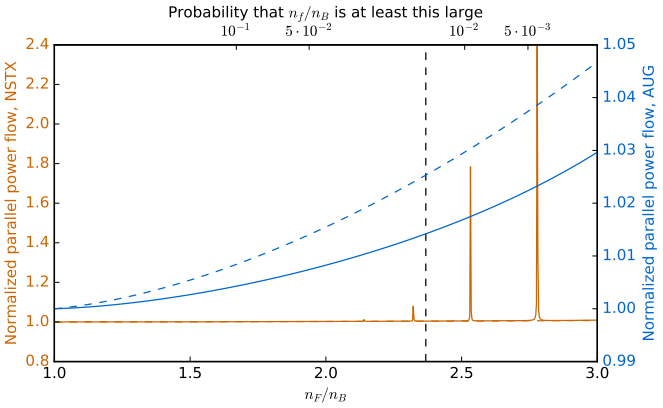

FIG. 15. Filament-integrated parallel RF power flow, normalized to that of the unperturbed case. All parameters except $k_\parallel$ are the same as in figure 10, but now $k_\parallel = 9\mathrm{m}^{-1}$ for NSTX (which is possible) and $k_\parallel = 3\mathrm{m}^{-1}$ for AUG (which may be achievable by changing the 3-strap antenna phasing). As expected, there are fewer mode conversion resonances, thinner and of far lower amplitude, at this higher $k_\parallel$ for NSTX, and still no mode conversion resonances for AUG. The secondary (top) x axis gives the cumulative distribution function for the density ratio (14). The vertical dashed line is the location of the fist resonance predicted by (22) for NSTX-like parameters.

D. Slow Waves, Fast Waves, and NSTX parallel RF power losses

The origin of the spurious parallel RF power flows in NSTX, which end up on the divertors, is observed[8,34] to be the entire SOL in front of the antenna, stretching from the antenna to the last closed flux surface. Proposed hypotheses to explain this spurious power redirection include both the hypothesis that it is due to propagating Fast Waves in the edge plasma[35], and the hypothesis that it is due to propagating Slow Waves in the edge plasma[36]. It is not clear that there is a region in the NSTX SOL where the Slow Wave is propagating at all, e.g. Green et al[21] find a density in NSTX that is everywhere too high for Slow Waves to propagate. In any case, Slow Waves certainly are not propagating in the entire SOL. Similarly, the Fast Wave is propagating in most of the SOL, but not within a few cm of the antenna[8]. So, neither the propagating-Slow-Wave-hypothesis, nor the propagating-Fast-Wave-hypothesis, naturally explain power redirection throughout the whole SOL.

The hypothesis of resonant wave-filament interaction that we argue for in this paper, on the other hand, naturally predicts the source of the redirected RF power to be the SOL in front of the antenna, between the antenna and the separatrix, which is precisely where the waves interact with filaments that end on the divertors.

V. CONCLUSION

In this paper we considered predictions regarding resonant ICRF wave-filament interactions in tokamak edge plasmas, based on analytic lines of reasoning such as the Mie series[1,2,6,7,9], and compared them with results of Finite Element calculations with a more realistic plasma filament waveform. Qualitatively, many of the analytic predictions remain valid in the more realistic cases considered here, especially those concerning the conditions under which mode conversion resonances are expected to be common (both the prediction that they occur under NSTX-like high harmonic fast wave conditions, and the prediction that they do not occur under AUG-like conditions, are confirmed numerically). Under these conditions, we find numerically that there are many more resonances than expected from analytic reasoning, but the density ratio n_F/n_B at which the first such resonance occurs is predicted approximately correctly by (22).

Clearly, mode conversion and mode conversion resonances due to filaments depend on sufficiently steep density gradients at the filament edge. But, under the conditions where we previously predicted mode conversion resonances to be important, that is low $k_\parallel$ and high harmonic heating (high $\frac{\omega}{\Omega_i}$), realistically sized and realistically sharp filaments are not in general smooth enough for mode conversion resonances to become negligible, not even for the smoothest Gaussian plasma filament waveforms.

ACKNOWLEDGMENTS

We acknowledge input from J.R. Myra (Lodestar Research Corporation), L. Colas (CEA), G. Suarez (IPP), and V. Bobkov (IPP).
This work has been carried out within the framework of the EUROfusion Consortium and has received funding from the Euratom research and training programme 2014-2018 and 2019-2020 under grant agreement No 633053. The views and opinions expressed herein do not necessarily reflect those of the European Commission.
The data that support the findings of this study are available from the corresponding author upon reasonable request.

[1] A. K. Ram and K. Hizanidis, "Scattering of radio frequency waves by cylindrical density filaments in tokamak plasmas," Physics of Plasmas **23**, 022504 (2016).
[2] W. Tierens, W. Zhang, and J. Myra, "Filament-assisted mode conversion in magnetized plasmas," Physics of Plasmas (2020).
[3] G. Mie, "Beiträge zur optik trüber medien, speziell kolloidaler metallösungen," Annalen der physik **330**, 377–445 (1908).
[4] G. Birkenmeier, P. Manz, D. Carralero, F. Laggner, G. Fuchert, K. Krieger, H. Maier, F. Reimold, K. Schmid, R. Dux, *et al.*, "Filament transport, warm ions and erosion in ASDEX Upgrade L-modes," Nuclear Fusion **55**, 033018 (2015).
[5] O. Garcia, "Blob transport in the plasma edge: a review," Plasma and Fusion Research **4**, 019–019 (2009).
[6] J. Myra and D. D'Ippolito, "Scattering of radio frequency waves by blob-filaments," Physics of Plasmas **17**, 102510 (2010).
[7] W. Zhang, W. Tierens, and M. Usoltceva, "Redirection of radio-frequency power flow by filaments," Nuclear Fusion (2020).
[8] R. Perkins, J. Hosea, G. Kramer, J.-W. Ahn, R. Bell, A. Diallo, S. Gerhardt, T. Gray, D. L. Green, E. F. Jaeger, *et al.*, "High-harmonic fast-wave power flow along magnetic field lines in the scrape-off layer of NSTX," Physical review letters **109**, 045001 (2012).
[9] S. Valvis, A. Ram, K. Hizanidis, P. Papagiannis, A. Papadopoulos, A. Zisis, I. Tigelis, and E. Glytsis, "Scattering of radio frequency waves by cylindrical filaments with general orientation relative to the magnetic field," Journal of Plasma Physics **84** (2018).
[10] D. D'ippolito, J. Myra, and S. Krasheninnikov, "Cross-field blob transport in tokamak scrape-off-layer plasmas," Physics of Plasmas **9**, 222–233 (2002).
[11] S. Krasheninnikov, D. D'ippolito, and J. Myra, "Recent theoretical progress in understanding coherent structures in edge and SOL turbulence," Journal of Plasma Physics **74**, 679–717 (2008).
[12] O. E. Garcia, R. Kube, A. Theodorsen, B. LaBombard, and J. Terry, "Intermittent fluctuations in the Alcator C-Mod scrape-off layer for ohmic and high confinement mode plasmas," Physics of Plasmas **25**, 056103 (2018).
[13] A. Theodorsen, O. E. Garcia, R. Kube, B. LaBombard, and J. L. Terry, "Relationship between frequency power spectra and intermittent, large-amplitude bursts in the Alcator C-mod scrape-off layer," Nuclear Fusion **57**, 114004 (2017).
[14] M. Jones, "On a class of distributions with simple exponential tails," Statistica Sinica , 1101–1110 (2008).
[15] S. Sugita, M. Yagi, S.-I. Itoh, and K. Itoh, "Propagation velocity analysis of a single blob in the SOL," Plasma and Fusion Research **3**, 040–040 (2008).
[16] A. Ross, A. Stegmeir, P. Manz, D. Groselj, W. Zholobenko, D. Coster, and F. Jenko, "On the nature of blob propagation and generation in the large plasma device: Global GRILLIX studies," Physics of Plasmas **26**, 102308 (2019).
[17] G. Yu, S. Krasheninnikov, and P. Guzdar, "Two-dimensional modelling of blob dynamics in tokamak edge plasmas," Physics of Plasmas **13**, 042508 (2006).
[18] Z. C. Ioannidis, A. K. Ram, K. Hizanidis, and I. G. Tigelis, "Computational studies on scattering of radio frequency waves by density filaments in fusion plasmas," Physics of Plasmas **24**, 102115 (2017).
[19] G. Birkenmeier, F. Laggner, M. Willensdorfer, T. Kobayashi, P. Manz, E. Wolfrum, D. Carralero, R. Fischer, B. Sieglin, G. Fuchert, *et al.*, "Magnetic field dependence of the blob dynamics in the edge of asdex upgrade l-mode plasmas," Plasma Physics and Controlled Fusion **56**, 075019 (2014).
[20] M. Campos Pinto and B. Després, "Constructive formulations of resonant maxwell's equations," SIAM Journal on Mathematical Analysis **49**, 3637–3670 (2017).
[21] D. L. Green, L. Berry, G. Chen, P. Ryan, J. Canik, and E. Jaeger, "Predicting high harmonic ion cyclotron heating efficiency in tokamak plasmas," Physical review letters **107**, 145001 (2011).
[22] "COMSOL, https://www.comsol.com/,".
[23] J. Jacquot, V. Bobkov, L. Colas, S. Heuraux, A. Křivská, L. Lu, J.-M. Noterdaeme, T. S. Team, and A. U. Team, "Full wave propagation modelling in view to integrated ICRH wave coupling/RF sheaths modelling," in *AIP Conference Proceedings*, Vol. 1689 (AIP Publishing, 2015) p. 050008.
[24] W. Tierens, D. Milanesio, G. Urbanczyk, W. Helou, V. V. Bobkov, J.-M. Noterdaeme, L. Colas, and R. Maggiora, "Validation of the ICRF antenna coupling code RAPLICASOL against TOPICA and experiments," Nuclear Fusion (2018).
[25] M. Usoltceva, R. Ochoukov, W. Tierens, A. Kostic, K. Crombé, S. Heuraux, and J. Noterdaeme, "Simulation of the ion cyclotron range of frequencies slow wave and the lower hybrid resonance in 3D in RAPLICASOL," Plasma Physics and Controlled Fusion **61**, 115011 (2019).
[26] T. H. Stix, *Waves in plasmas* (Springer Science & Business Media, 1992).
[27] L. Colas, J. Jacquot, J. Hillairet, W. Helou, W. Tierens, S. Heuraux, E. Faudot, L. Lu, and G. Urbanczyk, "Perfectly matched layers for time-harmonic transverse electric wave propagation in cylindrical and toroidal gyrotropic media," Journal of Computational Physics **389**, 94–110 (2019).
[28] V. Bobkov, D. Aguiam, R. Bilato, S. Brezinsek, L. Colas, H. Faugel, H. Fünfgelder, A. Herrmann, J. Jacquot, A. Kallenbach, *et al.*, "Making ICRF power compatible with a high-Z wall in ASDEX Upgrade," Plasma Physics and Controlled Fusion **59**, 014022 (2016).
[29] P. K. Kaw and J. McBride, "Surface waves on a plasma half-space," The Physics of Fluids **13**, 1784–1790 (1970).
[30] Y. M. Aliev, Y. M. Aliev, H. Schlüter, H. Schlüter, and A. Shivarova, *Guided-wave-produced plasmas*, Vol. 24 (Springer Science & Business Media, 2000).
[31] P. S. Epstein, "On the possibility of electromagnetic surface waves," Proceedings of the National Academy of Sciences of the United States of America **40**, 1158 (1954).
[32] J. Myra, personal communication.
[33] G. Harrer, E. Wolfrum, M. Dunne, P. Manz, M. Cavedon, P. Lang, B. Kurzan, T. Eich, B. Labit, J. Stober, *et al.*, "Parameter dependences of small edge localized modes (ELMs)," Nuclear Fusion **58**, 112001 (2018).
[34] R. Perkins, J.-W. Ahn, R. Bell, A. Diallo, S. Gerhardt, T. Gray, D. Green, E. Jaeger, J. Hosea, M. Jaworski, *et al.*, "Fast-wave power flow along sol field lines in nstx and the associated power deposition profile across the sol in front of the antenna," Nuclear Fusion **53**, 083025 (2013).
[35] N. Bertelli, E. Jaeger, J. Hosea, C. Phillips, L. Berry, P. Bonoli, S. Gerhardt, D. Green, B. LeBlanc, R. Perkins, *et al.*, "Full wave simulations of fast wave efficiency and power losses in the scrape-off layer of tokamak plasmas in mid/high harmonic and minority heating regimes," Nuclear Fusion **56**, 016019 (2015).
[36] D. Smithe and T. Jenkins, "Plasma in contact with metal:RF antenna near field behaviors in tokamaks," `https://apam.columbia.edu/files/seasdepts/applied-physics-and-applied-math/pdf-files/Smithe_Colloquium_06.pdf`, accessed: 11 April 2020.
[37] R. Maqueda, D. Stotler, and S. Zweben, "Intermittency in the scrape-off layer of the national spherical torus experiment during H-mode confinement," Journal of nuclear materials **415**, S459–S462 (2011).
[38] A. Messiaen and R. Weynants, "ICRH antenna coupling physics and optimum plasma edge density profile. application to ITER," Plasma Physics and Controlled Fusion **53**, 085020 (2011).
[39] A. Shivarova and I. Zhelyazkov, "Surface waves in a homogeneous plasma sharply bounded by a dielectric," Plasma Physics **20**, 1049 (1978).
[40] S. Zweben, R. Maqueda, D. Stotler, A. Keesee, J. Boedo, C. Bush, S. Kaye, B. LeBlanc, J. Lowrance, V. Mastrocola, *et al.*, "High-speed imaging of edge turbulence in NSTX," Nuclear Fusion **44**, 134 (2003).

Appendix A: A continuously differentiable generalisation of (6)

If desired, to make (6) have a continuous derivative while retaining the piecewise-exponential-like behaviour, we can introduce a third length scale δ_p (p for "peak") and convolve radially

$$n(r,\theta)_{\text{continuously differentiable}} = \frac{1}{\delta_p}\int_{r-\delta_p/2}^{r+\delta_p/2} n(r',\theta)_{\text{from (6)}}dr' \tag{A1}$$

The resulting expression is somewhat unwieldy, but still easily represented in terms of elementary functions. An example is shown in figure 16, and in figure 17 we see that the mode conversion resonances are not qualitatively different in this case.

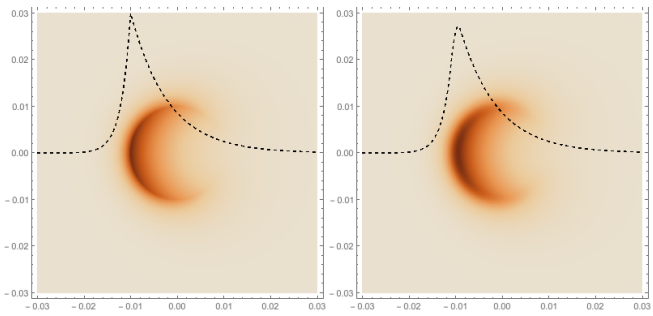

FIG. 16. A continuously differentiable generalisation of (6).

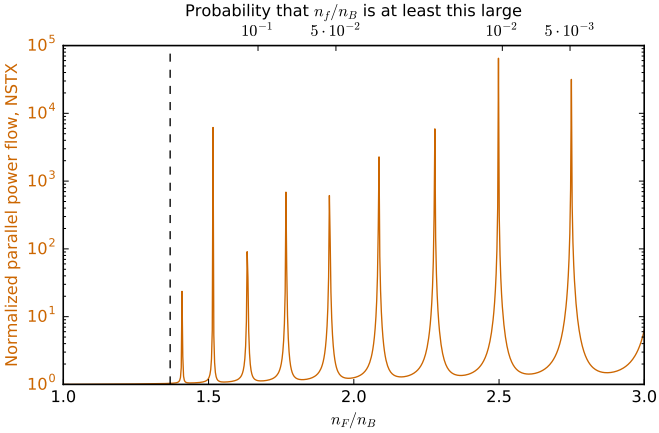

FIG. 17. The mode conversion resonances using the continuousely differentiable density (A1) are not qualitatively different from those with a density with a discontinuous derivative from figure 10. Here $\delta_p = \delta_r$.